ISA Transactions 95 (2019) 266–277

Contents lists available at ScienceDirect

ISA Transactions

journal homepage: www.elsevier.com/locate/isatrans

Practice article

Force ripple compensation in a PMLSM position servo system using periodic adaptive learning control

Wenjing Zhang [a,*], Nan Nan [a], Yifan Yang [a], Weifeng Zhong [a], YangQuan Chen [b]

[a] School of Electronic and Information Engineering, Beijing Jiaotong University, Beijing, 100044, PR China
[b] University of California, Merced, 5200 N. Lake Road, Merced, CA 95343, USA

HIGHLIGHTS

- An MRAC–PALC estimator for two dominant harmonic coefficients in the force ripple is proposed.
- The nature of the repetitive motion task is fully utilized.
- *A priori* knowledge is not required in the controller design.
- Improved force ripple compensation performance is demonstrated by simulations and experiments.

ARTICLE INFO

Article history:
Received 20 November 2018
Received in revised form 22 April 2019
Accepted 26 April 2019
Available online 4 May 2019

Keywords:
PMLSM position servo system
Force ripple compensation
Periodic adaptive learning control
Model reference adaptive control

ABSTRACT

Force ripple deteriorates the performance of permanent magnet linear synchronous motor (PMLSM) servo systems. Using a model reference adaptive control and periodic adaptive learning control (MRAC–PALC) algorithm, this paper presents a novel compensation method to eliminate the influence of force ripple on the system performance of a position servo system under repetitive motion tasks. The key idea of the proposed method is to utilize the periodic characteristics of both force ripple and system motion. The controller consists of four components: a PD component, a feedforward component, a velocity feedback component and an MRAC–PALC compensator. The first three components are designed in a conventional way. The compensator is divided into two parts: in the 0th-iteration, an MRAC algorithm is employed to obtain the initial information, and in the ith-iteration ($i \geq 1$), a PALC algorithm is used to learn from the information obtained in the previous period and update the controller parameters for estimating force ripple. Moreover, a theoretical stability analysis is given via Lyapunov stability theorem, and some comparative results are provided through simulations and experiments.

1. Introduction

PMLSM has received considerable attention because of many significant advantages such as lower thermal losses, higher torque to inertia ratio, superior power density, and most importantly, the ability to directly connect load to motor without a reducer. Force ripple is one of the most predominant nonlinear disturbances that degrade force smoothness and may lead to speed oscillations and stability problems [1], especially at a low velocity or with a relatively light load [2,3]. This paper proposes a novel compensation algorithm to eliminate the effect of force ripple on tracking performance of servo systems.

Force ripple sources can be divided into four main categories. First, in almost all motors with ferromagnetic core windings, mechanical construction primarily gives rise to ripples including reluctance force, cogging force and mutual force. Second, for a DC motor, ripple is generated from DC current sensor offset and D/A converter [4]. Third, in a servo system with a gear transmission mechanism, ripple comes from high-frequency load variations when the gears engage mutually. Finally, in some manufacturing and machining applications, ripple can result from external forces generated in a repetitive process at fundamental working frequency and its various harmonics. It is very interesting to note that force ripple can be regarded as a sinusoidal function, whose periodicity is only related to position and is independent of velocity, but its amplitude is determined by both position and velocity. Practically, ripple forms "bumps" along the motion direction, which are very difficult to eliminate completely [5].

There are two kinds of measures to suppress the impact of force ripple. An effective measure is to optimize motor structure [6]. Conversely, this approach will increase manufacturing complexity and lead to higher cost. On the other hand, motivated

* Corresponding author.
E-mail addresses: zhangwj@bjtu.edu.cn (W. Zhang), ychen53@ucmerced.edu (Y. Chen).

https://doi.org/10.1016/j.isatra.2019.04.032
0019-0578/

by the work in [7], considerable efforts have been focused on parameter identification methods in the force ripple model and corresponding compensation strategies. Based on the fact that force ripple can be expressed as a sum of a series of harmonics with respect to position, several identification techniques, including iterative learning [8], hysteretic relay [3] and closed-loop identification [9], have been developed to obtain the parameters in the force ripple model. In terms of compensation strategies, for the first category, the main idea is to design model-based controllers such as PID feedback controller with additional chatter [10] or dither [11], sliding mode controller [1], neural network controller [12] and intelligent optimization controller [13]. For the second category, ripple from DC offset is compensated by an internal model control method [4] and a fuzzy-logic control method [14]. For the last two categories, force ripple is considered as a part of the uncertainties and external disturbances and is addressed accordingly. Although the adaptive control method and its improved forms seem to be more popular [15,16], the amplitudes of force ripple model may fluctuate with velocity and load [8], making it difficult to completely compensate force ripple.

Moreover, approaches based on iterative learning control (ILC) have been receiving widespread acceptance. A PALC compensation scheme is given to minimize the state-dependent cogging effect [17], and a periodic learning disturbance observer-based method is proposed to eliminate force ripple and other disturbances [18]. Additionally, a repetitive learning variable structure control method is proposed to minimize periodic speed ripple in a PMSM and two ILC schemes and their modified forms are presented to suppress the speed and torque ripples in a PMLSM, respectively [8,19]. However, force ripple frequency, which is fixed and can be obtained accurately, is not fully utilized.

Under repetitive tasks, force ripple behaves periodically, and two coefficients of the dominant harmonic are time-varying. It is obvious that force ripple and system motion share some common features, and accordingly, the periodic control approach has a greater advantage than its conventional counterparts. In reality, it is not difficult to find many such cases: for example, cutter's motion in manufacturing [1], maglev train operation, and gait and joint flexion-extension of a rehabilitation robot. Thus, the goal of this paper is to consider the inherent periodicity of both force ripple and reference signal and design an MRAC–PALC strategy to eliminate the influence of force ripple.

Motivated by several outstanding achievements in [17,20,21], through analysis of force ripple properties using fast Fourier transform (FFT), a new MRAC–PALC compensation method is proposed to eliminate parasitic force ripple in a class of position servo systems under repetitive motion tasks. The key point of the algorithm is to estimate the amplitudes of force ripple with a periodic adaptive estimator and add an extra control effort to accurately compensate force ripple. The proposed MRAC–PALC algorithm consists of a PD component for global stability and robustness, a feedforward component for fast response, a velocity feedback component for damping improvement and an MRAC–PALC compensator component for accurate estimation of force ripple amplitudes.

In summary, comparing with present force ripple compensation methodologies, the main contributions of this paper are listed as follows.

(1) Dynamic characteristics of force ripple are fully utilized by using position-dependent harmonics model, enhancing the compensation effect. In contrast, force ripple is only regarded as a part of the lumped disturbance in present PALC suppression methods [15,17].

(2) Two time-varying and periodic coefficients of the dominant harmonic are estimated by the PALC algorithm under repetitive tasks. The advantage of this estimation method is that force ripple is accurately approximated at any time in each period. Existing adaptive compensation algorithms do not consider the nature of periodic tasks [2,20,21].

(3) *A priori* knowledge is not needed in the proposed MRAC–PALC approach, and all parameters can be acquired through adaptive learning. Therefore, some problems resulting from initial values are avoided.

(4) Using the fixed dominant harmonic frequency of force ripple identified by FFT, implementation complexity of the control algorithm is reduced.

This paper is organized as follows. In Section 2, a PMLSM position servo system with a force ripple disturbance is briefly introduced. In Section 3, using FFT, the spectrum of force ripple is analyzed, and the dominant harmonic frequency is identified. In Section 4, a control algorithm with a uniform format and two sets of different adaptation laws is discussed. In Section 5, simulation and experimental results are given to verify the effectiveness of the proposed approach. Finally, the conclusions are presented in Section 6.

2. Problem formulation

In this paper, a typical three-phase PMLSM position servo system with force ripple is considered. For simplicity and without loss of generality, the following assumptions are first made: (1) the core is unsaturated, (2) the eddy current and hysteretic loss are negligible, and (3) electromotive force (EMF) is sinusoidal. Using a field-oriented control strategy, d-axis current is regulated to be zero.

Taking force ripple into account, the servo system is modeled by

$$\dot{x} = \frac{K_f u_q - (L_q s + R)F_{\text{ripple}}}{L_q M s^2 + MRs + \frac{\pi}{\tau_p} K_f \lambda_f p_n}, \tag{1}$$

$$K_f = \frac{3\pi}{2\tau_p} p_n \lambda_f, \tag{2}$$

where x is displacement of PMLSM motor, u_q is q-axis stator voltage, L_q is q-axis inductance, R is stator resistance, p_n is the number of pole pairs, τ_p is pole pitch, λ_f is flux linkage, M is the mass of mover, K_f is force coefficient, and F_{ripple} is force ripple disturbance. At the same time, x is assumed to be bounded and second-order differentiable. Ignoring the effect of q-axis inductance L_q, (1) can be simplified as

$$M\ddot{x} = \frac{K_f}{R} u_q - \frac{\pi p_n \lambda_f K_f}{\tau_p R} \dot{x} - F_{\text{ripple}}, \tag{3}$$

Let us define

$$m = \frac{MR}{K_f}, a = -\frac{\pi p_n \lambda_f}{\tau_p}, F_r = \frac{R}{K_f} F_{\text{ripple}}.$$

Thus, we have

$$m\ddot{x} = a\dot{x} + u_q - F_r. \tag{4}$$

Let u_q be denoted by u as controller effort; then, (4) can be rewritten as

$$v(t) = \dot{x}(t), \tag{5}$$

$$m\dot{v}(t) = av(t) + u(t) - F_r, \tag{6}$$

In our study, force ripple is modeled as

$$F_r = \sum_{n=1}^{n_{\max}} A_{rn} \sin(n\omega_0 x + \varphi_n). \tag{7}$$

where ω_0 is the fundamental frequency and is regarded as a constant, and A_{rn} and φ_n are the magnitude and phase angle of the nth-order force ripple harmonic, respectively.

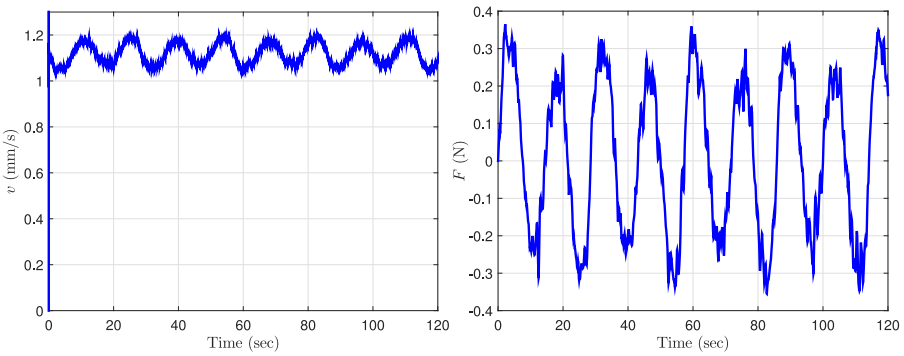

Fig. 1. Measured system velocity and output force when PMLSM moves at 1 mm/s.

Our goal is to design an MRAC–PALC estimator to approximate force ripple under repetitive motion tasks and eliminate the position and velocity tracking errors. Throughout the paper, the following assumptions hold:

Assumption 2.1. For a given servo system, operating conditions and system dynamics are significantly undiversified.

Assumption 2.2. The desired position trajectory is periodic.

Assumption 2.3. In each iteration, both time instant and present position are acquired accurately in both iteration domain i and time domain t.

Assumption 2.4. The influences of force ripple on the servo system in different iterations are nearly identical.

It can be seen that the above assumptions hold under repetitive motion tasks. Further, the desired and actual position trajectories, corresponding velocities and force ripple have the following two properties:

Property 2.1. *From Assumptions 2.1–2.3, assuming that a good tracking performance is achieved, the desired position trajectory x_d and all measured system states share fixed periodic time P_t. Furthermore, P_t can be acquired exactly. Thus, we can obtain*

$$x_d(t+iP_t)=x_d(t),\ v_d(t+iP_t)=v_d(t),$$
$$x(t+iP_t)\approx x(t),\ v(t+iP_t)\approx v(t).$$

Property 2.2. *From Assumption 2.4 and Property 2.1, since the period of desired trajectory $x_d(t)$ is fixed as P_t and force ripple $F_r(t)$ consists of many harmonics with respect to $x(t)$, we have*

$$F_r(t+iP_t)\approx F_r(t).$$

3. Dominant harmonic frequency identification in force ripple

Since force ripple is described as a position-dependent function that consists of many harmonics, it is natural to identify the amplitudes and frequencies of these harmonics, especially dominant harmonic frequency. Although the amplitude identification has been proven to be cumbersome [1], harmonic frequencies can be obtained through spectrum analysis [22], especially FFT.

As to the series on the right-hand side of (7), based on motor structure and corresponding parameters, fundamental ripple frequency ω_0 with respect to displacement x can be determined as

$$\omega_0=\pi/\tau_p, \tag{8}$$

Then, (7) can be rewritten as

$$\begin{aligned}F_r&=\sum_{n=1}^{n_{\max}}A_{rn}\sin\left(\frac{n\pi}{\tau_p}x+\varphi_n\right)\\&=\sum_{n=1}^{n_{\max}}A_{r1n}\cos\left(\frac{n\pi}{\tau_p}x\right)+\sum_{n=1}^{n_{\max}}A_{r2n}\sin\left(\frac{n\pi}{\tau_p}x\right).\end{aligned} \tag{9}$$

When the servo system moves at a very low and constant velocity, $\dot{v}_d=0$ and $\dot{v}\approx 0$; then, (6) can be changed as

$$av+u-F_r\approx 0. \tag{10}$$

Theoretically, the difference between the frequency spectra of measured effort output u and force ripple F_r is only frequency component FFT[av]. When the servo system moves at a very low and constant velocity, av is very small, and F_r is very close to u, making it possible to obtain the features of F_r by analyzing u. Due to disturbances and other uncertainties, it is difficult to keep v absolutely stable, resulting in spectrum errors. However, a relatively accurate frequency spectrum of F_r can be obtained through that of u.

To observe force ripple and acquire the dominant harmonic frequency, an open-loop experiment at a very low and constant velocity is performed, where velocity $v=1$ mm/s, and running time is 120 s. The measured system velocity and output force are shown in Fig. 1, and the frequency spectrum of force ripple is shown in Fig. 2. It is obvious that fluctuations exist in the measured velocity due to inherent force ripple.

From (8), the fundamental ripple frequency $\omega_0=\pi/\tau_p=0.196$ rad/mm. Considering $x=vt$, the fundamental ripple frequency f_0 with respect to time t is $f_0=\omega_0 v/(2\pi)=0.0313$ Hz. From Fig. 2, it is apparent that the fundamental frequency is 0.033 Hz, the second harmonic ($f=0.066$ Hz) is the dominant component, and other harmonics are less significant because their amplitudes are less than 10% of the dominant one. Hence, for the dominant harmonic, $n=2$ and $\omega_r\doteq n\pi v/\tau_p=0.3927$ rad/s. Note that a slight difference exists between the computed and measured fundamental frequencies. Here, only the dominant frequency component is considered, and (9) is simplified as

$$F_r=A_{r1}\cos(\omega_r x)+A_{r2}\sin(\omega_r x). \tag{11}$$

where two amplitudes, A_{r1} and A_{r2}, can be different. Based on this simplified model, an MRAC–PALC compensation algorithm is presented to eliminate the influence of force ripple on servo system performance.

From Property 2.2, we have

$$A_{r1}(t+iP_t)=A_{r1}(t),\ A_{r2}(t+iP_t)=A_{r2}(t). \tag{12}$$

Apparently, it is crucial to find accurate estimations of $\hat{A}_{r1}$ and $\hat{A}_{r2}$ for A_{r1} and A_{r2}, respectively, such that an additional control

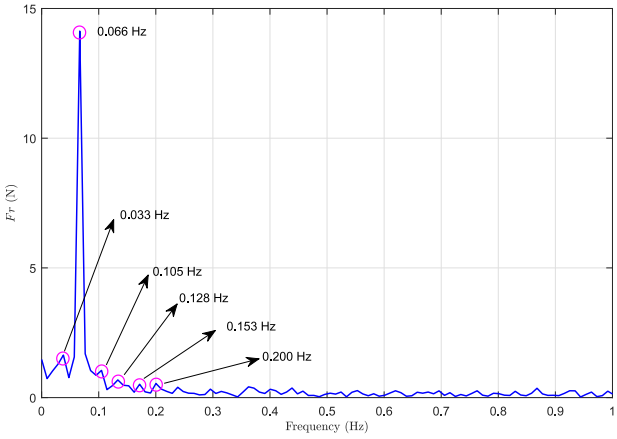

Fig. 2. Frequency spectrum of the force ripple when PMLSM moves at 1 mm/s.

effort u_r can be generated to eliminate the estimated force ripple $\hat{F}_r =: \hat{A}_{r1}\cos(\omega_r x) + \hat{A}_{r2}\sin(\omega_r x)$. Note that a more accurate dominant harmonic frequency may be obtained by combining FFT method with other identification approaches [23].

4. Design of MRAC–PALC controller

In this section, the proposed MRAC–PALC compensation algorithm is illustrated in detail. First, a controller frame with a uniform format is given. Then, two sets of different adaptation laws for the 0th-iteration and ith-iteration ($i \geq 1$) are presented. At the same time, the asymptotic stability of the proposed scheme is analyzed via Lyapunov stability theorem.

4.1. MRAC–PALC-Based controller design

To begin with, we assume that desired position x_d, desired velocity v_d and its derivative $\dot{v}_d$ are all bounded. Here, control errors are given as

$$e_x = x_d - x, \tag{13}$$

$$e = \dot{e}_x + \lambda e_x, \tag{14}$$

where λ is a positive constant to be designed.

Then, the following estimation errors are defined

$$\tilde{A}_{r1} = A_{r1} - \hat{A}_{r1},\ \tilde{A}_{r2} = A_{r2} - \hat{A}_{r2}.$$

To eliminate the influence of force ripple on system performance, the proposed MRAC–PALC control law is constructed as

$$u = cme + \lambda m e_v - av + m\dot{v}_d + \hat{A}_{r1}\cos(\omega_r x) + \hat{A}_{r2}\sin(\omega_r x). \tag{15}$$

where c is a positive coefficient to be regulated, v_d is desired velocity, $v_d = \dot{x}_d$, and $e_v = v_d - v$.

From (15), it can be seen that, according to mechanism, the control law is divided into four parts: part one ($cme + \lambda m e_v$) acts as a conventional linear PD controller, part two ($-av$) is a velocity feedback controller that can increase the damping characteristics and enhance the tracking performance, the third part ($m\dot{v}_d$) is a feedforward controller that can improve transient performance and avoid using high-gain feedback, and the last adaptive compensator ($u_r \doteq \hat{A}_{r1}\cos(\omega_r x) + \hat{A}_{r2}\sin(\omega_r x)$) is updated by different adaptation laws and used to eliminate the estimated force ripple $\hat{F}_r$ in real time.

From (14), when $\lambda > 0$, the error transfer function $G_e(s) = \frac{e_x(s)}{e(s)} = \frac{1}{s+\lambda}$ is always stable. Furthermore, if e exponentially converges to a very small value or zero, e_x also converges. Thus, another goal of this paper is to minimize e to achieve high-performance position and velocity tracking.

The schematic diagram of the MRAC–PALC scheme is shown in Fig. 3.

4.2. Design of MRAC-based adaptation laws (0th-iteration)

In the 0th-iteration (i.e., the first time period), to guarantee system stability, the adaptation laws for MRAC component are designed as

$$\dot{\hat{A}}_{r1} = k_{10} e \cos(\omega_r x), \tag{16}$$

$$\dot{\hat{A}}_{r2} = k_{20} e \sin(\omega_r x). \tag{17}$$

where k_{10} and k_{20} are positive adaptation gains to be designed.

Theorem 4.1. *Suppose that $|v_d(t)|$ is bounded; let $e_x(0) = e(0) = 0$. Considering the position servo system (5), (6) with force ripple (11) and the control goal of tracking desired position trajectory x_d and its derivative v_d, the employment of the control law given by (15) with MRAC adaptation laws presented by (16) and (17) ensures that e_x and e are bounded in l_2-norm when $t < P_1$.*

Proof. Please refer to Appendix A for the proof of the theorem. □

Remark 4.1. *In practice, the main task of MRAC is to ensure system stability in the 0th-iteration. Thus, small values of k_{10} and k_{20} are feasible to achieve this goal.*

4.3. Design of PALC-based adaptation laws (ith-iteration)

From the 1st-iteration (the second time period) and onwards (i.e., $t \geq P_1$ and $i \geq 1$), the coefficients of first three linear parts in the control law (15) are the same as those in the 0th-iteration. To learn from the information in the previous period, update the parameters in force ripple model and ensure asymptotical stability of the servo system. The designed periodic adaptation laws for the PALC compensator are given as

$$\hat{A}_{r1}(t) - \hat{A}_{r1}(t - P_t) = \frac{k_{1i}}{m}[e_v(t) + \lambda e_x(t)]\cos(\omega_r x), \tag{18}$$

$$\hat{A}_{r2}(t) - \hat{A}_{r2}(t - P_t) = \frac{k_{2i}}{m}[e_v(t) + \lambda e_x(t)]\sin(\omega_r x). \tag{19}$$

where both k_{1i} and k_{2i} are positive periodic adaptive learning gains to be regulated.

Theorem 4.2. *Suppose that $|v_d(t)|$ is bounded. From the 1st-iteration period and onwards, considering the position servo system (5), (6) with force ripple (11) and the control goal of tracking the desired position trajectory x_d and its derivative v_d, the employment of the nonlinear control law given by (15) with PALC adaptation laws presented by (18), (19) ensures that the system (5), (6) is asymptotically stable, and the position tracking error (13) converges to zero as $t, i \to \infty$.*

Proof. Please see Appendix B for the proof of the theorem. □

From (18), (19), we can see that $\hat{A}_{r1}$ and $\hat{A}_{r2}$ can be acquired at any time in each period, and together with ω_r identified through FFT, force ripple can be estimated in real time.

In the 1st-iteration, the stored information in the 0th-iteration period acts as an initial condition. Therefore, no *a priori* knowledge is needed to activate the PALC algorithm. From the 2^{nd}-iteration on ($i \geq 2$), estimated amplitudes $\hat{A}_{r1}$ and $\hat{A}_{r2}$ of force

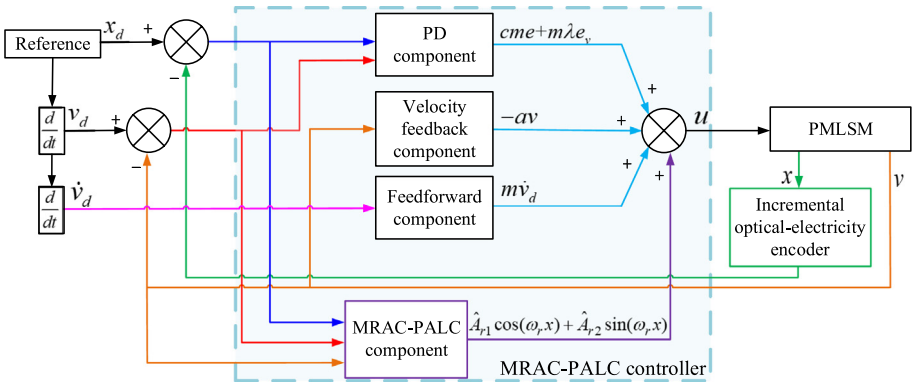

Fig. 3. Block diagram of the MRAC–PALC controller.

Table 1
PMLSM parameters.

PMLSM parameters	X-axis	Y-axis
Mass of the motor M (kg)	0.58	0.76
Stator resistance R (Ω)	10.7	18.2
Force coefficient K_f (N/A)	54.5	97.5
Pole pitch τ_p (mm)	16	16
Number of pole pairs p_n	6	6
q-axis inductance L_q (mH)	3.8	6.3
Flux linkage λ_f (Wb)	0.031	0.055
Continuous thrust F_c (N)	109	145
Peak thrust (1 s) F_p (N)	327	435

Table 2
PD gains.

Definitions	Symbols	Values
PD gains of C3 for X-axis	k_P, k_D	215508, 0.0003
PD gains of C3 for Y-axis	k_P, k_D	229406, 0.0012
PD gains of C1 and C2 for X-axis	c, λ	7516,211
PD gains of C1 and C2 for Y-axis	c, λ	8226,211

Table 3
Adaptation gains.

Definitions	Symbols	Values
Adaptation gains of C1 for X-axis	$k_{10}, k_{20}, k_{1i}, k_{2i}$	0.3, 0.1, 178, 185
Adaptation gains of C1 for Y-axis	$k_{10}, k_{20}, k_{1i}, k_{2i}$	0.2, 0.1, 197, 186
Adaptation gains of C2 for X-axis	k_1, k_2	121,109
Adaptation gains of C2 for Y-axis	k_1, k_2	101,115

ripple in the previous $(i-1)$th-iteration are utilized as the information to be learned in the present ith-iteration. In contrast with conventional PID and adaptive controllers, a larger memory is indispensable in the implementation of the proposed MRAC–PALC algorithm. However, more information that is stored for updating the adaptation laws, more potential the proposed method possesses to enhance tracking performance. Therefore, a tradeoff between memory size and expected tracking performance has to be made in the controller implementation.

5. Comparative simulation and experimental results

In this section, the proposed MRAC–PALC compensation algorithm for force ripple is investigated through simulations and experiments. The compensation effects of the proposed MRAC–PALC controller (C1), an MRAC controller (C2) and a PD controller (C3) are compared from some different aspects. In addition, some related frequency spectra and ITAE results are presented to highlight the superiority of the proposed approach.

5.1. Experimental setup

As shown in Fig. 4, the gantry system LMG2A-CB6-CC8 with two PMLSM-driven axes (X and Y), manufactured by Hiwin™, is used in our experiments. A programmable multi-axis controller (PMAC), produced by Delta Tau Data Systems Inc., is employed to control two PMLSMs. A MATLAB™-based software development kit and a Links-Box real-time simulator developed by Beijing LINKS™ Co. are used to simulate and generate controller code for PMAC. Other main components include two motor D1 drivers made by Mega-Fabs Motion Systems Ltd., a DTC-8B interface board produced by Delta Tau Data Systems Inc., and a power supply. PMLSM parameters are listed in Table 1.

5.2. Tuning of controller parameters

To make a fair comparison and illustrate the performance improvement of the servo system with the proposed MRAC–PALC algorithm, all gains of three controllers are chosen to achieve best tracking performance, the tuning procedure is separated into two steps below.

Step 1: Design of PD gains

The gain tuning of C3 and PD components of C1 and C2 can be achieved easily. Here, using MATLAB™ Toolbox and making a tradeoff between overshoot and settling time, PD gains are given in Table 2.

Step 2: Selection of adaptation gains

For adaptation gains of MRAC and PALC, in theory, we can choose all real numbers that are greater than zero. The adaptation gains are increased gradually from very small values, improving convergence rate and minimizing position tracking errors. However, high adaptation gains may lead to oscillation and even instability. Considering the stability, convergence rate and motion smoothness, through repeated experiments (trial and error), the adaptation gains of C1 and C2 are shown in Table 3.

5.3. Simulation studies

To show the superiority and effectiveness of the proposed MRAC–PALC compensation algorithm, some comparative tracking simulations for X-axis and Y-axis are conducted with Links-Box simulator. P_t is fixed as 2 s, and sample time $T = 10^{-5}$ s. The desired sinusoidal position trajectory is selected as $x_d(t) = 0.15\sin(\pi t)$ m. For the proposed MRAC–PALC scheme, the MRAC algorithm is employed to guarantee stability in the 0th-iteration, and the PALC algorithm is not yet added. From the 1st-iteration on, MRAC is replaced by PALC to update amplitude parameters

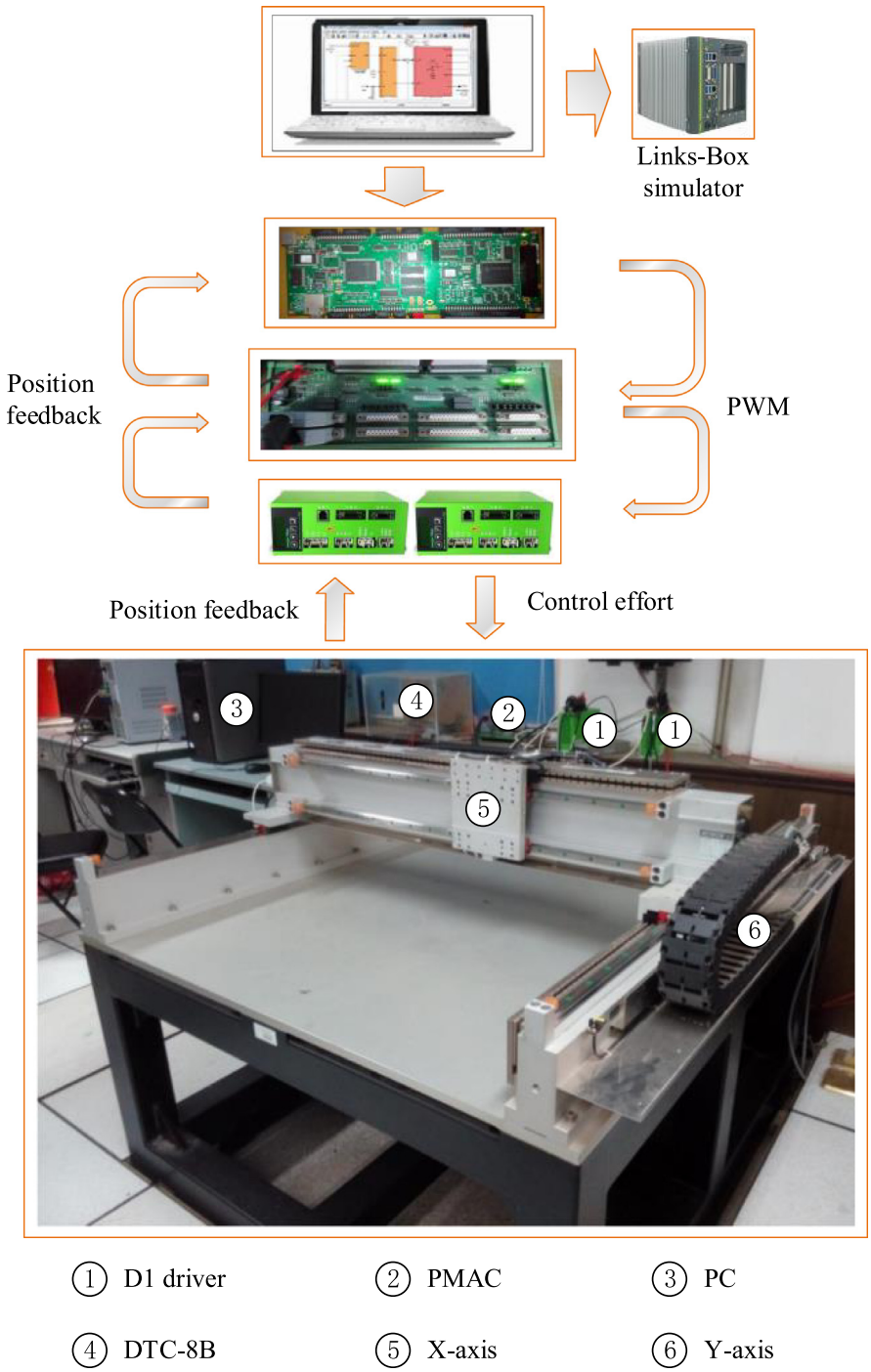

Fig. 4. Block diagram and data flows of the testbed.

of force ripple from information in the previous period. Note that, in all figures below, (a) and (b) represent *X*-axis and *Y*-axis, respectively.

To simulate the influence of force ripple on system performance, based on (9) and the identification results of force ripple in Section 3, two force ripple disturbance signals are modeled as position-dependent multiple harmonics, as shown in Table 4.

Fig. 5 shows a comparison of position tracking errors when three controllers are used. It can be observed clearly that, without compensation under C3, maximum position tracking errors are about 83 μm (X-axis) and 140 μm (Y-axis). After adaptive compensation under C2, maximum position tracking errors of about 0.52 μm (X-axis) and 0.58 μm (Y-axis) are achieved. In contrast, with C1, maximum position tracking errors are only about 0.06 μm (X-axis) and 0.02 μm (Y-axis) after 6 iterations. To be noted, the peak of tracking errors decreases very fast as the iteration increases. Due to utilizing periodic information hidden in repetitive tasks, the proposed MRAC–PALC algorithm exhibits a much better tracking performance than MRAC algorithm.

Figs. 6 and 7 show velocity tracking and tracking errors with three controllers, and the corresponding maximum velocity tracking errors are shown in Table 5. It can be seen that the proposed MRAC–PALC algorithm can achieve smoother velocity tracking than C2 and C3.

Table 4
Magnitudes of the harmonics for simulating force ripple disturbance.

Definitions	Harmonic frequencies	Harmonic magnitudes
Harmonics for X-axis	$\frac{\pi}{\tau}, \frac{2\pi}{\tau}, \frac{3\pi}{\tau}, \frac{4\pi}{\tau}, \frac{5\pi}{\tau}, \frac{6\pi}{\tau}$	0.05,0.45,0.04,0.031,0.022,0.035
Harmonics for Y-axis	$\frac{\pi}{\tau}, \frac{2\pi}{\tau}, \frac{3\pi}{\tau}, \frac{4\pi}{\tau}, \frac{5\pi}{\tau}, \frac{6\pi}{\tau}$	0.1,0.8,0.08,0.061,0.042,0.055

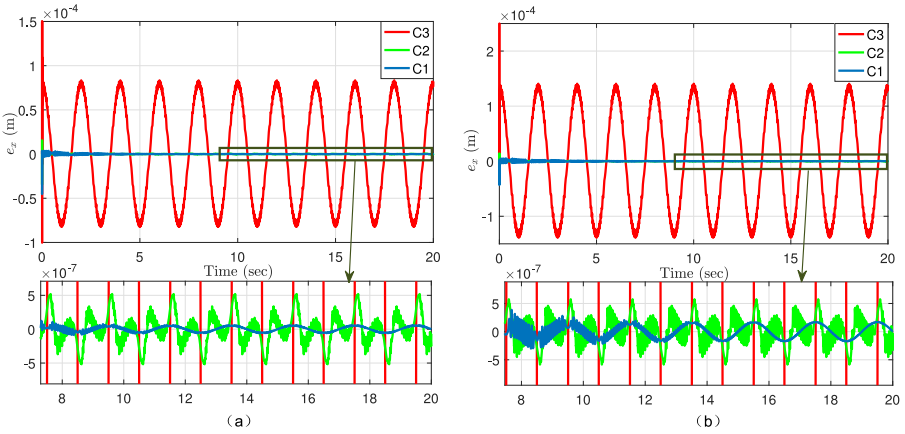

Fig. 5. Position tracking errors from MRAC–PALC (C1), MRAC (C2) and PD controller (C3).

Table 5
Maximum velocity tracking errors with three controllers in the simulation.

Definitions	X-axis (m/s)	Y-axis (m/s)
Maximum velocity tracking error with C1	1.3×10^{-5}	3.7×10^{-5}
Maximum velocity tracking error with C2	7.5×10^{-5}	1×10^{-4}
Maximum velocity tracking error with C3	1.96×10^{-4}	5.25×10^{-4}

Table 6
Maximum tracking errors with three controllers.

Controllers	Position errors (μm)		Velocity errors (m/s)	
	X-axis	Y-axis	X-axis	Y-axis
C1	1.2	1.0	8.1×10^{-4}	8.6×10^{-4}
C2	3.1	2.7	1.9×10^{-3}	1.5×10^{-3}
C3	82	142	1.6×10^{-2}	1.3×10^{-2}

Fig. 8 shows a comparison of control efforts used in C1 and C3. From the plots, we can easily see that control effort of the proposed MRAC–PALC controller is very close to that of C3. Therefore, we can conclude that the proposed MRAC–PALC controller only requires a very small additional control effort over conventional PD controller to compensate force ripple disturbance.

The desired and estimated force ripple trajectories are shown in Fig. 9, and the updating processes of estimated coefficients of $\hat{A}_{r1}$ and $\hat{A}_{r2}$ are shown in Fig. 10. We can see clearly that both $\hat{A}_{r1}$ and $\hat{A}_{r2}$ behave periodically under repetitive motion tasks, and the given force ripple is approximated successfully by the proposed MRAC–PALC algorithm after only about 6 iterations. At the same time, the proposed MRAC–PALC algorithm performs better than MRAC algorithm in both convergence rate and estimation accuracy.

5.4. Experimental investigations

To further demonstrate the effectiveness of the proposed MRAC–PALC approach, a line-shaped contour following task is carried out, and desired position trajectory for both X and Y axes is chosen as $x_d(t) = 0.15\sin(\pi t)$ m.

The position tracking trajectories with three different controllers are shown in Fig. 11, the position and velocity tracking errors are given in Fig. 12 and Fig. 13, respectively, and the corresponding tracking errors are shown in Table 6. It can be seen that, similar to simulation results, tracking performance of the proposed MRAC–PALC method is better than those of MRAC and PD methods. Moreover, due to relatively slight load, the motion of one axis has little influence on the motion of the other.

To investigate the performance of servo system and its frequency content, FFT is applied to position errors and control efforts under three controllers, and the corresponding results are shown in Figs. 14 and 15, respectively. We can see that, with the proposed MRAC–PALC algorithm, the position error spectrum in low frequency range is appreciably attenuated, verifying the effectiveness and superiority of the proposed compensation algorithm. Meanwhile, the FFT results of control efforts under three controllers are very similar, indicating again that only a slight extra control effort is required to achieve force ripple elimination.

To further evaluate the superiority of the proposed MRAC–PALC method over conventional MRAC and PD algorithms, the tracking performances with three controllers are compared in terms of ITAE, as reported in Fig. 16. It is obvious that the proposed MRAC–PALC method performs better than other two methods.

6. Conclusions

In this paper, a novel MRAC–PALC compensation algorithm is proposed to eliminate force ripple in position tracking systems under repetitive motion tasks. In this method, a uniform controller with two sets of different adaptation laws is given. The MRAC algorithm is used to ensure system stability in the 0th-iteration and obtain initial information, and the PALC algorithm is employed to guarantee the asymptotic stability of servo system and tracking performance from the 1st-iteration and onwards. Compared with conventional compensation methods, the proposed scheme combines the periodic characteristics of system motion and inherent force ripple and makes use of the merits of MRAC and PALC. From simulation and experimental results, we can see clearly that the proposed MRAC–PALC scheme works effectively, performs better than conventional PD and MRAC algorithms, and significantly eliminates force ripple. Furthermore, the proposed MRAC–PALC control strategy in this paper can be

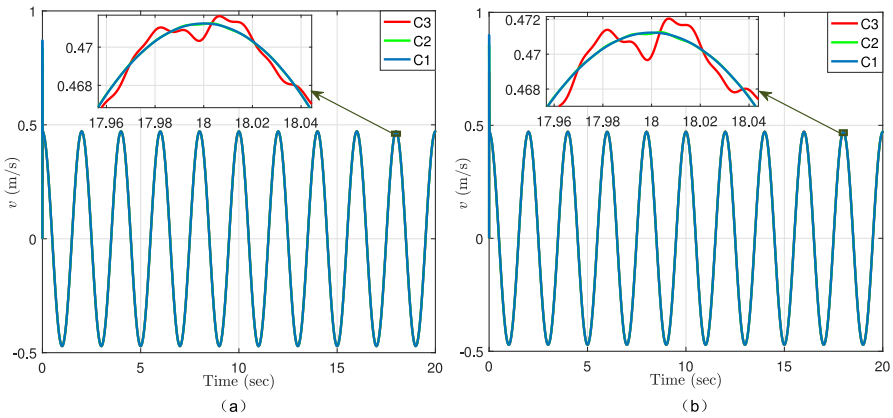

Fig. 6. Velocity tracking trajectories from MRAC–PALC (C1), MRAC (C2) and PD controller (C3).

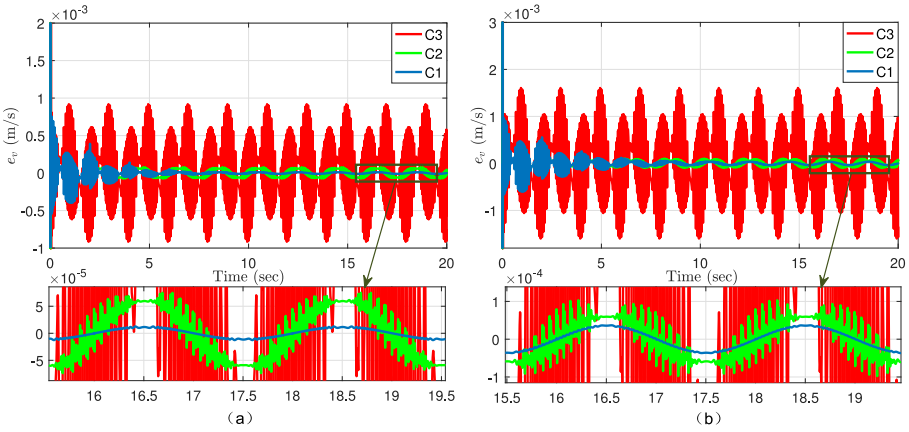

Fig. 7. Velocity tracking errors from MRAC–PALC (C1), MRAC (C2) and PD controller (C3).

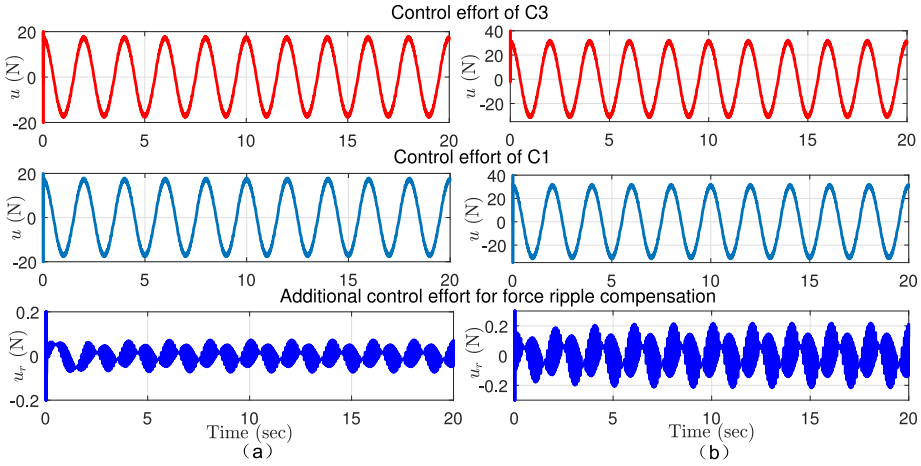

Fig. 8. Control efforts from MRAC–PALC (C1) and PD controller (C3) and additional control effort for force ripple compensation.

employed to compensate other periodic disturbances in servo systems under repetitive motion tasks.

Future investigations can introduce optimal parameter selection strategies into the proposed MRAC–PALC algorithm to improve convergence rate. Although implementation complexity increases, tracking performance may be further improved.

Acknowledgments

This work is supported in part by National Key R&D Program of China under Grants 2016YFB1200601 and 2016YFB1200602 and in part by National Aerospace Science Foundation of China under Grant 201501M5001. Authors would also like to appreciate the anonymous reviewers and in particular, Deputy Editor-in-Chief, Prof. WANG QG, for their valuable review comments and suggestions. Authors are grateful to Dr. Xiangbin Liu in Beijing Jiaotong University for providing gantry system LMG2A-CB6-CC8 for the experiments.

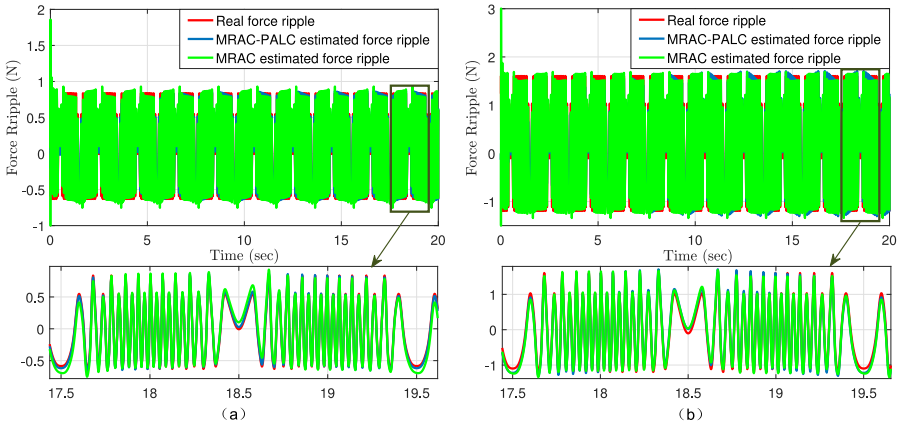

Fig. 9. Actual and estimated force ripple with MRAC–PALC and MRAC methods.

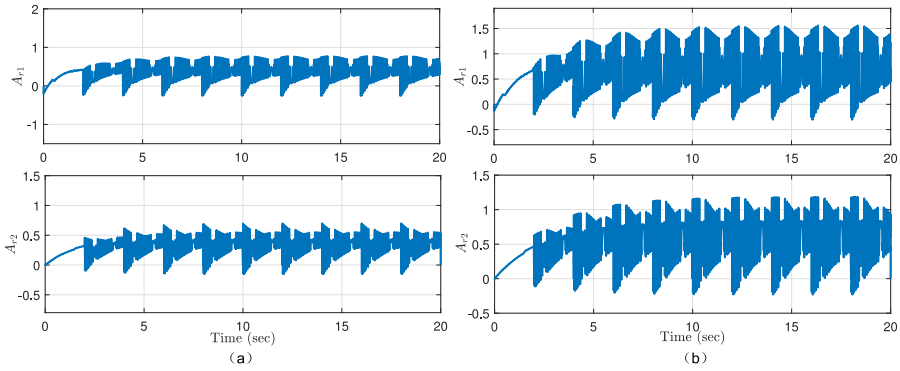

Fig. 10. Adaptation process of the force ripple parameters with MRAC–PALC controller.

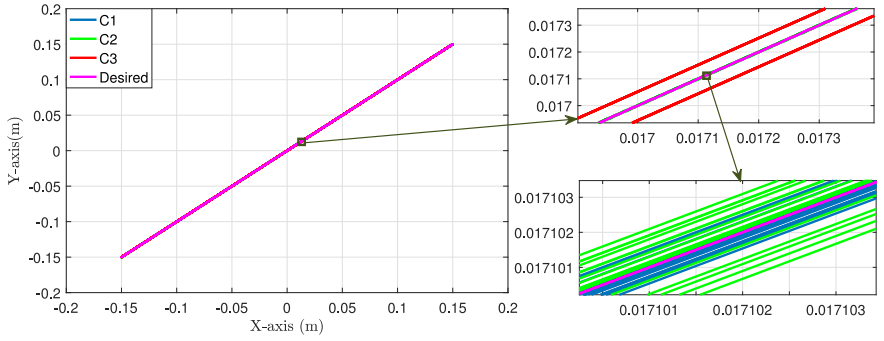

Fig. 11. Experimental position tracking trajectories of the double axes from MRAC–PALC (C1), MRAC (C2) and PD controller (C3).

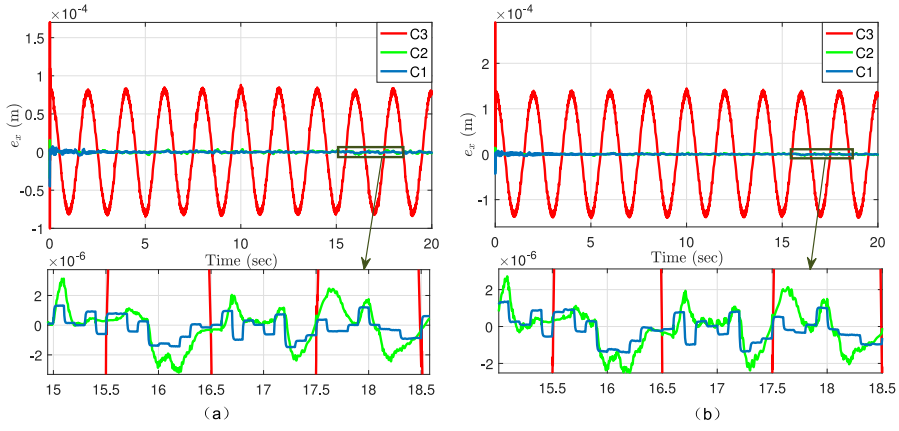

Fig. 12. Experimental position tracking errors from MRAC–PALC (C1), MRAC (C2) and PD controller (C3).

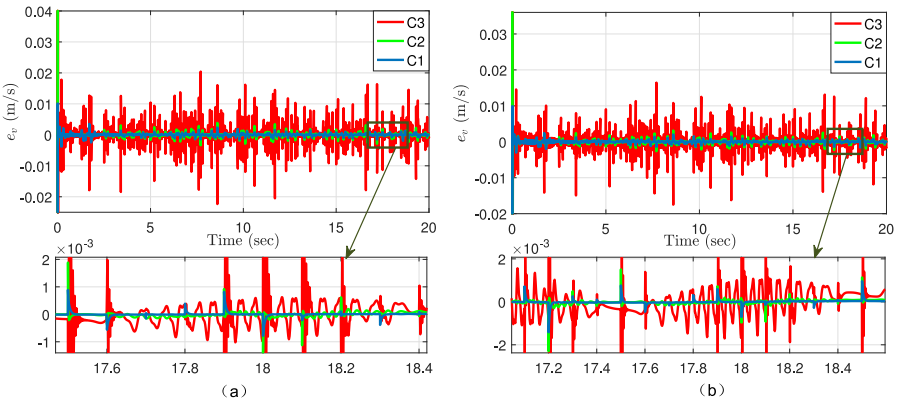

Fig. 13. Experimental velocity tracking errors from MRAC–PALC (C1), MRAC (C2) and PD controller (C3).

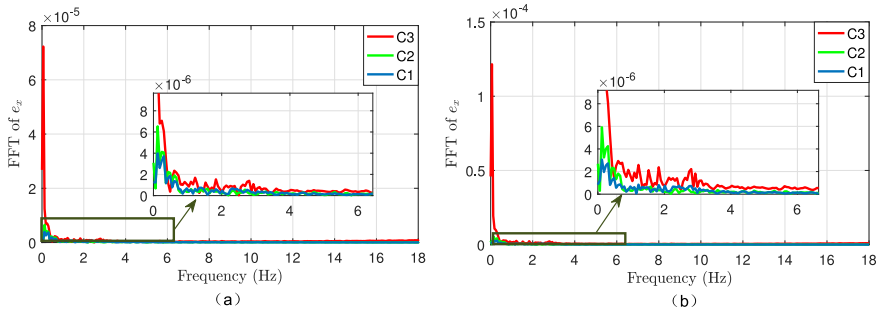

Fig. 14. FFT of the position tracking errors from MRAC–PALC (C1), MRAC (C2) and PD controller (C3).

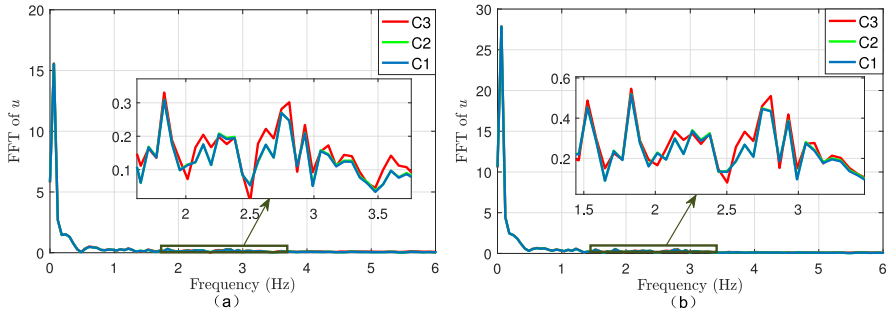

Fig. 15. FFT of the control efforts from MRAC–PALC (C1), MRAC (C2) and PD controller (C3).

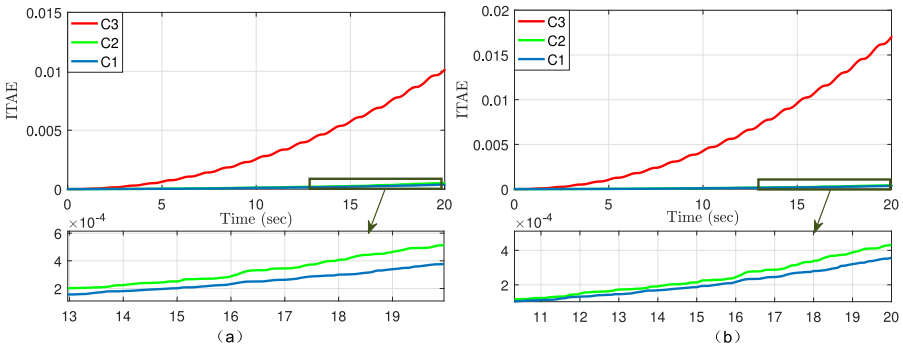

Fig. 16. ITAE of MRAC–PALC (C1), MRAC (C2) and PD controller (C3).

Declaration of competing interest

The authors declare that they have no known competing financial interests or personal relationships that could have appeared to influence the work reported in this paper.

Appendix A. Proof of Theorem 4.1

In the 0th-iteration, choose a Lyapunov function candidate $V(t)$ as

$$V(t)=\frac{1}{2}me^2+\frac{1}{2k_{10}}\tilde{A}_{r1}^2+\frac{1}{2k_{20}}\tilde{A}_{r2}^2, \tag{20}$$

Taking the derivative of V with respect to time t yields

$$\dot{V}=me\dot{e}+\frac{1}{k_{10}}\tilde{A}_{r1}\dot{\tilde{A}}_{r1}+\frac{1}{k_{20}}\tilde{A}_{r2}\dot{\tilde{A}}_{r2}, \tag{21}$$

Substituting (6), (11), (14), (15) and e_v into (21), we have

$$\dot{V}=-cme^2+\tilde{A}_{r1}[e\cos(\omega_r x)+\frac{1}{k_{10}}\dot{\tilde{A}}_{r1}]+\tilde{A}_{r2}[e\sin(\omega_r x)+\frac{1}{k_{20}}\dot{\tilde{A}}_{r2}], \tag{22}$$

Inserting the adaptation laws (16) and (17) into (22), $\dot{V}$ becomes

$$\dot{V}=-cme^2\le 0. \tag{23}$$

Since $c>0$ and $m>0$, $\dot{V}$ is negative-definite, and only $e=:\dot{e}_x+\lambda e_x=0$ makes $\dot{V}=0$; the equilibrium at $e=0$ is asymptotically stable. Then, both $e\to 0$ and $e_x\to 0$ can be achieved as $t\to\infty$.

Further, it is reasonable to say that V is bounded. In the first period ($t\le P_t$), when $e(0)=0$, $e_x(0)=0$ and $|v(t)|$ is bounded, both e and e_x are bounded in l_2-norm.

The proof is completed. □

Appendix B. Proof of Theorem 4.2

From the 1st-iteration and onwards, choose a Lyapunov-like function candidate as

$$V(t)=\frac{1}{2}[e(t)]^2+\frac{1}{2k_{1i}}\int_{t-P_t}^{t}\tilde{A}_{r1}^2(\tau)d\tau+\frac{1}{2k_{2i}}\int_{t-P_t}^{t}\tilde{A}_{r2}^2(\tau)d\tau, \tag{24}$$

In order to satisfy Lyapunov stability theorem, the difference of V between two discrete time points t (in the present ith-iteration) and t–P_t (in the previous (i–1)th-iteration) is defined as

$$\begin{aligned}\Delta V(t)=&V(t)-V(t-P_t)\\=&\frac{1}{2}[e_v(t)+\lambda e_x(t)]^2-\frac{1}{2}[e_v(t-P_t)+\lambda e_x(t-P_t)]^2+\\&\frac{1}{2k_{1i}}\int_{t-P_t}^{t}[\tilde{A}_{r1}^2(\tau)-\tilde{A}_{r1}^2(\tau-P_t)]d\tau+\\&\frac{1}{2k_{2i}}\int_{t-P_t}^{t}[\tilde{A}_{r2}^2(\tau)-\tilde{A}_{r2}^2(\tau-P_t)]d\tau\\=&\int_{t-P_t}^{t}e[\dot{e}_v(\tau)+\lambda\dot{e}_x(\tau)]d\tau+\\&\frac{1}{2k_{1i}}\int_{t-P_t}^{t}[\tilde{A}_{r1}^2(\tau)-\tilde{A}_{r1}^2(\tau-P_t)]d\tau+\\&\frac{1}{2k_{2i}}\int_{t-P_t}^{t}[\tilde{A}_{r2}^2(\tau)-\tilde{A}_{r2}^2(\tau-P_t)]d\tau.\end{aligned} \tag{25}$$

To write the above equation more concisely, the terms on the right-hand side in (25) are separated into following three parts

$$A(t)=\int_{t-P_t}^{t}e[\dot{e}_v(\tau)+\lambda\dot{e}_x]d\tau, \tag{26}$$

$$B(t)=\frac{1}{2k_{1i}}\int_{t-P_t}^{t}[\tilde{A}_{r1}^2(\tau)-\tilde{A}_{r1}^2(\tau-P_t)]d\tau, \tag{27}$$

$$C(t)=\frac{1}{2k_{2i}}\int_{t-P_t}^{t}[\tilde{A}_{r2}^2(\tau)-\tilde{A}_{r2}^2(\tau-P_t)]d\tau, \tag{28}$$

Then, (25) is rewritten as

$$\Delta V(t)=A(t)+B(t)+C(t). \tag{29}$$

From (6) and (13), we have

$$\dot{e}_v=\dot{v}_d-\frac{1}{m}[av-A_{r1}cos(\omega_r x)-A_{r2}sin(\omega_r x)+u], \tag{30}$$

Inserting (15) and (30) into (26) yields

$$A(t)=\int_{t-P_t}^{t}\{-ce^2+\frac{1}{m}e[\tilde{A}_{r1}cos(\omega_r x)+\tilde{A}_{r2}sin(\omega_r x)]\}d\tau, \tag{31}$$

$B(t)$ is deduced as

$$\begin{aligned}B(t)=&\frac{1}{2k_{1i}}\int_{t-P_t}^{t}[\tilde{A}_{r1}^2(\tau)-\tilde{A}_{r1}^2(\tau-P_t)]d\tau\\=&\frac{1}{2k_{1i}}\int_{t-P_t}^{t}\{[A_{r1}(\tau)-\hat{A}_{r1}(\tau)]^2-\\&[A_{r1}(\tau-P_t)-\hat{A}_{r1}(\tau-P_t)]^2\}d\tau\\=&\frac{1}{2k_{1i}}\int_{t-P_t}^{t}[\hat{A}_{r1}(\tau-P_t)-\hat{A}_{r1}(\tau)]\\&\{2[A_{r1}(\tau)-\hat{A}_{r1}(\tau)]+[\hat{A}_{r1}(\tau)-\hat{A}_{r1}(\tau-P_t)]\}d\tau,\end{aligned} \tag{32}$$

Letting $\beta(t)=\hat{A}_{r1}(t)-\hat{A}_{r1}(t-P_t)$, the above equation is rewritten as

$$B(t)=-\frac{1}{2k_{1i}}\int_{t-P_t}^{t}\beta(\tau)\{2[A_{r1}(\tau)-\hat{A}_{r1}(\tau)]+\beta(\tau)\}d\tau, \tag{33}$$

Similarly, letting $\gamma(t)=\hat{A}_{r2}(t)-\hat{A}_{r2}(t-P_t)$, $C(t)$ is deduced as

$$C(t)=-\frac{1}{2k_{2i}}\int_{t-P_t}^{t}\gamma(\tau)\{2[A_{r2}(\tau)-\hat{A}_{r2}(\tau)]+\gamma(\tau)\}d\tau, \tag{34}$$

With a substitution from (31), (33) and (34) and rearranging the terms of $\Delta V(t)$, we obtain

$$\begin{aligned}\Delta V(t)=&\int_{t-P_t}^{t}\{-ce^2-\frac{1}{2k_{1i}}\beta^2(\tau)-\frac{1}{2k_{2i}}\gamma^2(\tau)\}d\tau\\&+\int_{t-P_t}^{t}\{\frac{e}{m}[\tilde{A}_{r1}cos(\omega_r x)+\tilde{A}_{r2}sin(\omega_r x)]\\&-\frac{\tilde{A}_{r1}}{k_{1i}}\beta(\tau)-\frac{\tilde{A}_{r2}}{k_{2i}}\gamma(\tau)\}d\tau,\end{aligned} \tag{35}$$

Inserting the PALC adaptation laws (18) and (19) into the above equation, it follows that

$$\begin{aligned}\Delta V(t)=&\int_{t-P_t}^{t}\{-ce^2-\frac{1}{2k_{1i}}\beta^2(\tau)-\frac{1}{2k_{2i}}\gamma^2(\tau)\}d\tau\\=&\int_{t-P_t}^{t}\{-[c+\frac{k_{1i}cos^2(\omega_r x)+k_{2i}sin^2(\omega_r x)}{2m^2}]e^2\}d\tau\\\le&-c\int_{t-P_t}^{t}e^2d\tau,\end{aligned} \tag{36}$$

Note that c is a positive design coefficient, and we have

$$\Delta V(t)\le 0. \tag{37}$$

Since $\Delta V(t)=0$ if and only if $e\equiv 0$. According to Lyapunov stability theorem, we can conclude that both $\hat{A}_{r1}$ and $\hat{A}_{r2}$ are bounded with respect to time t. Thus, e is asymptotically stable

and converges to zero. Furthermore, position tracking error $e_x \rightarrow 0$ is achieved as $i \rightarrow \infty$. This means that with the proposed control law (15) and the PALC adaptation laws (18), (19), both the stability and tracking convergence of the servo system can be guaranteed.

The proof is completed. □

References

[1] Sencer B, Shamoto E. Effective torque ripple compensation in feed drive systems based on the adaptive sliding-mode controller. IEEE/ASME Trans Mechatronics 2014;19(6):1764–72.

[2] Zhao S, Tan K. Adaptive feedforward compensation of force ripples in linear motors. Control Eng Pract 2005;13(9):1081–92.

[3] Chen SL, Tan KK, Huang S, Teo CS. Modeling and compensation of ripples and friction in permanent-magnet linear motor using a hysteretic relay. IEEE/ASME Trans Mechatronics 2010;15(4):586–94.

[4] Gan WC, Qiu L. Torque and velocity ripple elimination of AC permanent magnet motor control systems using the internal model principle. IEEE/ASME Trans Mechatronics 2004;9(2):436–47.

[5] Fang J, Zhou X, Liu G. Instantaneous torque control of small inductance brushless DC motor. IEEE Trans Power Electron 2012;27(12):4952–64.

[6] Wang M, Li L, Pan D. Detent force compensation for PMLSM systems based on structural design and control method combination. IEEE Trans Ind Electron 2015;62(11):6845–54.

[7] Röhrig C, Jochheim A. Identification and compensation of force ripple in linear permanent magnet motors. In: Proceedings of the 2001 American Control Conference. vol. 3; 2001, p. 0743-1619.

[8] Qian W, Panda SK, Xu J-X. Torque ripple minimization in PM synchronous motors using iterative learning control. IEEE Trans Power Electron 2004;19(2):272–9.

[9] Bascetta L, Rocco P, Magnani G. Force ripple compensation in linear motors based on closed-loop position-dependent identification. IEEE/ASME Trans Mechatronics 2010;15(3):349–59.

[10] Zhao S, Putra A, Tan K, Panda S, Lee T. Intelligent compensation of friction, ripple, and hysteresis via a regulated chatter. ISA Trans 2006;45(3):419–33.

[11] Tan K, Chin S, Dou H. Feedforward suppression of force ripple based on a simplex-optimized dither signal. ISA Trans 2003;42(1):19–27.

[12] Heydarzadeh M, Rezaei S, Azizi N, Kamali AE. Compensation of friction and force ripples in the estimation of cutting forces by neural networks. Measurement 2018;114:354–64.

[13] Lai C, Feng G, Iyer KLV, Mukherjee K, Kar NC. Genetic algorithm-based current optimization for torque ripple reduction of interior PMSMs. IEEE Trans Ind Appl 2017;53(5):4493–503.

[14] Uddin MN. An adaptive-filter-based torque-ripple minimization of a fuzzy-logic controller for speed control of IPM motor drives. IEEE Trans Ind Appl 2011;47(1):350–8.

[15] Cho K, Kim J, Choi SB, Oh S. A high-precision motion control based on a periodic adaptive disturbance observer in a PMLSM. IEEE/ASME Trans Mechatronics 2015;20(5):2158–71.

[16] Prathibanandhi K, Ramesh R. Hybrid control technique for minimizing the torque ripple of brushless direct current motor. Measur Control 2018;51(7–8):321–35.

[17] Luo Y, Chen Y, Pi Y. Cogging effect minimization in PMSM position servo system using dual high-order periodic adaptive learning compensation. ISA Trans 2010;49(4):479–88.

[18] Cho K, Nam K. Periodic learning disturbance observer based precision motion control in PMLSM motion systems considering long-term instability problem. Int J Precis Eng Manuf 2016;17(9):1101–12.

[19] Qian W, Panda SK, Xu JX. Speed ripple minimization in PM synchronous motor using iterative learning control. IEEE Trans Energy Convers 2005;20(1):53–61.

[20] Tan K, Lee T, Dou H, Zhao S. Force ripple suppression in iron-core permanent magnet linear motors using an adaptive dither. J Franklin Inst B 2004;341(4):375–90.

[21] Tan KK, Huang SN, Lee TH. Robust adaptive numerical compensation for friction and force ripple in permanent-magnet linear motors. IEEE Trans Magn 2002;38(1):221–8.

[22] Wang M, Li L, Pan D, Tang Y, Guo Q. High-bandwidth and strong robust current regulation for PMLSM drives considering thrust ripple. IEEE Trans Power Electron 2016;31(9):6646–57.

[23] Wan Z, Wang T, Li S, Zhang Z. A modified particle filter for parameter identification with unknown inputs. Struct Control Health Monit 2018;25(12). e2268.